ARTICLE OPEN

Check for updates

Integration of body-mounted ultrasoft organic solar cell on cyborg insects with intact mobility

Yujiro Kakei[1,2], Shumpei Katayama[1,3], Shinyoung Lee[1], Masahito Takakuwa[1,3], Kazuya Furusawa[4], Shinjiro Umezu[2,3], Hirotaka Sato[5], Kenjiro Fukuda[1,6]✉ and Takao Someya[1,6,7]✉

Cyborg insects have been proposed for applications such as urban search and rescue. Body-mounted energy-harvesting devices are critical for expanding the range of activity and functionality of cyborg insects. However, their power outputs are limited to less than 1 mW, which is considerably lower than those required for wireless locomotion control. The area and load of the energy harvesting device considerably impair the mobility of tiny robots. Here, we describe the integration of an ultrasoft organic solar cell module on cyborg insects that preserves their motion abilities. Our quantified system design strategy, developed using a combination of ultrathin film electronics and an adhesive–nonadhesive interleaving structure to perform basic insect motion, successfully achieved the fundamental locomotion of traversing and self-righting. The body-mounted ultrathin organic solar cell module achieves a power output of 17.2 mW. We demonstrate its feasibility by displaying the recharging wireless locomotion control of cyborg insects.

npj Flexible Electronics (2022)6:78 ; https://doi.org/10.1038/s41528-022-00207-2

INTRODUCTION

Cyborgs, which are integrations of machines and organisms, can be used not only to substitute an organism's defective body parts, but also to realise functions that exceed the organism's normal capabilities[1]. Advancements in electronics have resulted in the increasing integration of organisms and machines. The miniaturisation and fabrication of low-power consumption semiconducting chips through micro/nanofabrication have resulted in small-organism cyborgs. In particular, cyborg insects with small integrated circuits to control their behaviour have been proposed for applications such as urban search and rescue, environmental monitoring, and inspection of dangerous areas[2–7]. The integration of thin and soft electronics into organisms can improve their ease of use in numerous applications[8–11]. Stretchable electronics enable the integration of devices on three-dimensional curved surfaces with movable joints[12,13].

The evolution of electronics that can be integrated with organisms has increased the demand for the development of power supply devices with higher power densities. The volume and weight limitations of batteries for untethered robots can be overcome using recharging strategies such as having robots return to designated recharging locations before their batteries run out[14] and supplying power to batteries wirelessly[15,16]. An energy-harvesting device mounted on a robot can expand its range of activities[17,18]. A biofuel cell that generates power from an insect's body is a promising energy-harvesting device[19]. To date, 333 μW is the highest output power achieved with enzymatic biofuel cells. Battery charging and circuit driving have been achieved for this power output for walking cockroaches[20,21].

Advanced functions, such as the wireless locomotion control of cyborg insects, require energy-harvesting devices that can generate several milliwatts or higher. A solar cell can generate 10 mW cm^{-2} or higher power under outdoor sunlight conditions; this technology can generate the highest power output available under outdoor conditions[22]. A rigid silicon solar cell mounted on an immovable insect is used to charge lithium–polymer batteries[23,24]. Emergent solar cells, including organic[25], perovskite[26], and quantum dot cells[27], can achieve high power per weight because of their reduced substrate and passivation thicknesses, which is beneficial for achieving integration in living small insects. Ultrathin organic solar cells having a total thickness of less than 5 μm can achieve a power conversion efficiency (PCE) of 15.8% resulting in a power per weight of 33.8 W g^{-1} [28].

However, achieving a power output of 10 mW or higher using energy harvesters mounted on living movable insects for wireless locomotion control remains challenging. To integrate devices into small animals with limited surface areas and carry loads[29], device design and integration strategy of large-area solar cells is required to obtain sufficient power output and simultaneously maintain the basic behavioural abilities of insects. Because the output power of the solar cell is proportional to the area, both the load of the device and the contact between the device and the moving joints considerably impair motion abilities.

In this article, we report a power-rechargeable cyborg insect that uses a mounted ultrasoft organic solar cell module that does not impair the insect's basic motion abilities, and demonstrate recharging wireless locomotion control with all components integrated on insects. A combination of ultrathin film electronics and an adhesive–nonadhesive interleaving structure on the insect abdomen exhibited a success rate of greater than 80% in self-righting attempts. The effect of film attachment on the basic motion was quantified using an approximated buckling load model. An ultrathin organic solar cell module achieved a power output of 17.2 mW on the curved abdomen of the insect,

[1]Center for Emergent Matter Science, RIKEN, 2-1 Hirosawa, Wako, Saitama 351-0198, Japan. [2]Department of Integrative Bioscience and Biomedical Engineering, Center for Advanced Biomedical Sciences, TWIns Waseda Univerisity, 2-2 Wakamatsu-cho, Shinjuku-ku, Tokyo 162-8480, Japan. [3]Department of Modern Mechanical Engineering, Waseda University, 3-4-1 Okubo, Shinjuku-ku, Tokyo 169-8555, Japan. [4]Department of Applied Chemistry and Food Science, Faculty of Environmental and Information Sciences, Fukui University of Technology, 3-6-1 Gakuen, Fukui 910-8505, Japan. [5]School of Mechanical and Aerospace Engineering, Nanyang Technological University, N3.2 – 01- 20, 65 Nanyang Drive, Singapore 637460, Singapore. [6]Thin-Film Device Laboratory, RIKEN, 2-1 Hirosawa, Wako, Saitama 351-0198, Japan. [7]Electrical and Electronic Engineering and Information Systems, The University of Tokyo, 7-3-1 Hongo, Bunkyo-ku, Tokyo 113-8656, Japan. ✉email: kenjiro.fukuda@riken.jp; someya@ee.t.u-tokyo.ac.jp

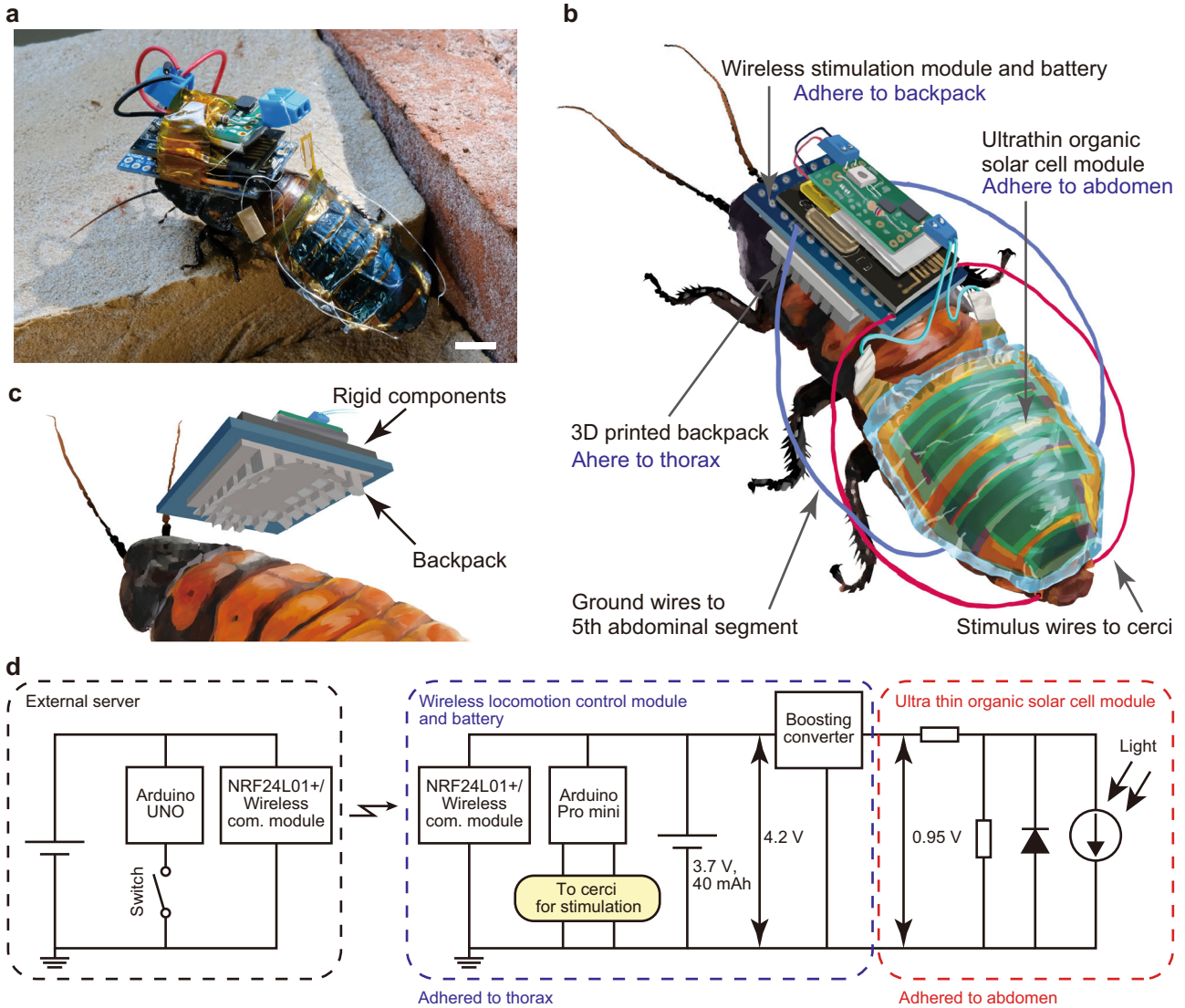

Fig. 1 Rechargeable cyborg insects with an ultrasoft organic solar cell module. a Photograph of a cyborg insect using *G. portentosa*. Scale bar, 10 mm. **b** Schematics of cyborgs. **c** Schematics of mounting rigid components onto the thorax with the assistance of a 3D-printed backpack. **d** Circuit diagram of the system of the wireless locomotion control module and rechargeable power sources.

which charged a lithium polymer battery to operate the wireless locomotion control module.

RESULTS AND DISCUSSION

Structure of the rechargeable cyborg insect

Gromphadorhina portentosa (*G. portentosa*, Madagascar hissing cockroach) was used in this study. Electronic components were mounted on the dorsal side of the insect (Fig. 1a, b). A wireless locomotion control module consisting of wireless communication circuits, stimulation voltage controller circuits, boosting circuits, and a lithium–polymer battery was mounted on the thorax with the support of a three-dimensional (3D)-printed soft backpack that followed the curved surface of the thorax (Fig. 1c). A 4 μm thick organic solar cell module was attached to the abdomen. The power generated by the ultrathin organic solar cell under simulated sunlight (100 mW cm^{-2}) was boosted to 4.2 V by using a boosting circuit to charge the battery, and the battery supplied power to the wireless locomotion control module. Locomotion control signals were transferred wirelessly from the external server using Bluetooth (Fig. 1d). Stimulation signals were applied to the cerci through wires to wirelessly control locomotion of the insect (Supplementary Fig. 1). Cerci are paired appendages on the rearmost segments of the abdomen. When electrical stimulation was applied to the right cercus, the insect made the turn-right locomotion and vice versa.

A soft backpack that fits perfectly on curved surfaces stabilised mount components on the thorax. The backpack was designed using a precise 3D model of *G. portentosa* (Supplementary Fig. 2), and 3D printed with an elastic polymer. The columnar structure at the bottom matches the curved surface shape (Fig. 1c, Supplementary Fig. 3). Owing to the soft material and columnar structure, the backpack designed using the design extracted from an individual insect can tolerate the difference in shape existing between individual insects and make good adhesion (Supplementary Fig. 4). The adhesion of the backpack attached to the thorax was secured even after a month in the breeding environment, which confirmed that the backpack adhered to the body for the long term. By contrast, the adhesion between rigid components using the conventional adhesion method using beeswax delaminated from the thorax after 30 min in ambient room temperature (approximately 20 °C)[2].

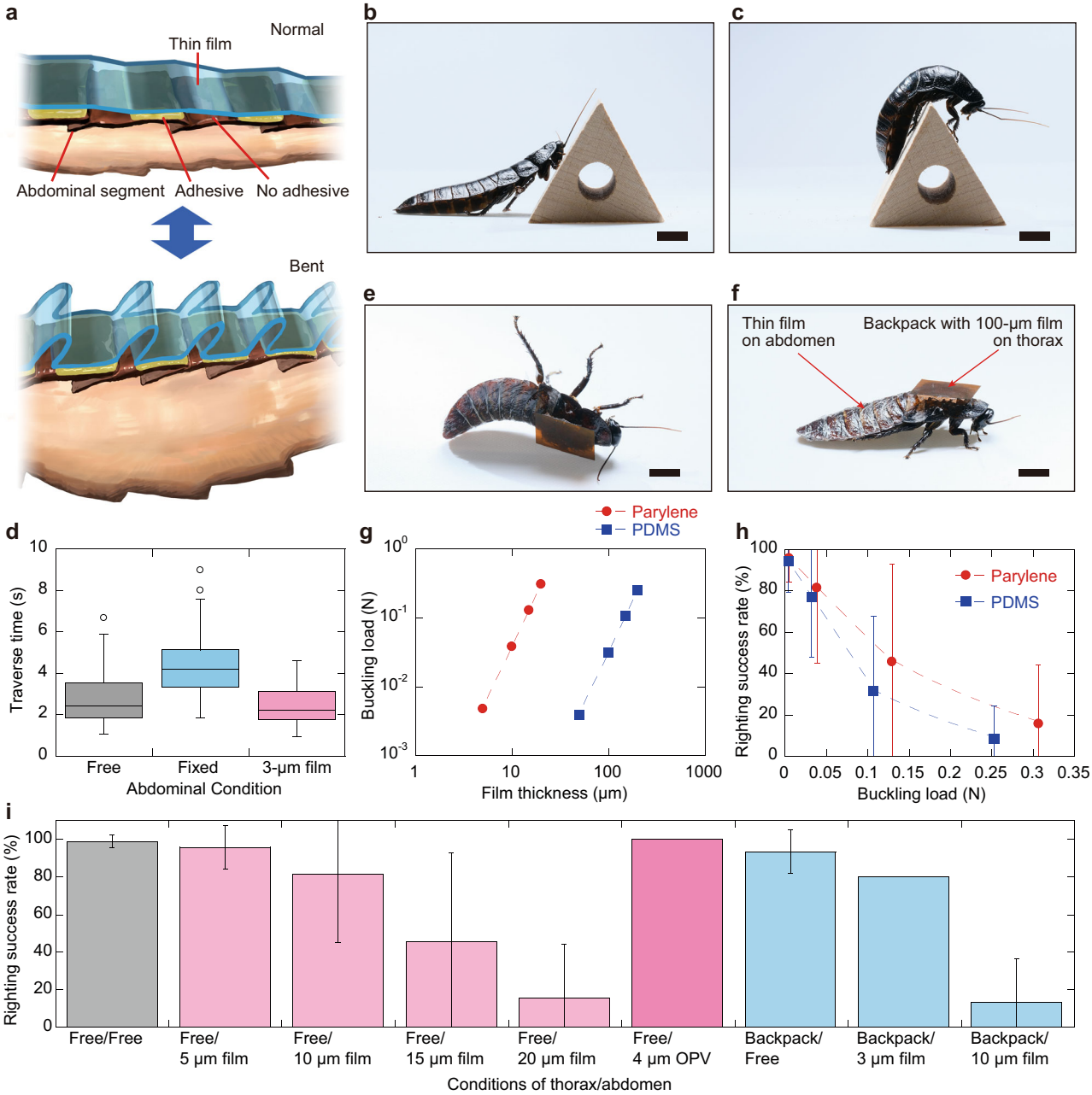

Fig. 2 Fundamental behavioural ability with electronics. a Schematic cross-sectional illustration of abdominal segments with thin films attached using an adhesive-nonadhesive interleaving structure. The interleaving structure enables outward bending of the thin films during the deformation of the abdomen. **b**, **c** Images of traversing the obstacle near the starting point (**b**) and near the end point (**c**). Scale bars, 10 mm. **d** Box-plots of traversing time under various abdominal conditions. Left: free condition with no film, Centre: abdomen is fixed with a thick film, Right: 3 μm thick parylene film was adhered onto the abdomen with interleaving structure. Center line, median; box limits, upper and lower quartiles; whiskers, 1.5x interquartile range; points, outliers. **e**, **f** Photographs of the self-righting attempt while the insect was upside-down (**e**) and after a successful attempt (**f**). Scale bars, 10 mm. **g** Calculated buckling load of the films attached to the abdomen as a function of the film thickness. Red circles and blue squares represent the parylene film ($E = 4.0$ GPa) and PDMS film ($E = 3.3$ MPa), respectively. **h** Righting success rate as a function of the buckling load. Red circles and blue squares represent parylene and PDMS film. **i** Righting success rate for various thoracic and abdominal conditions. The error bars in **h**, and **i** represent the standard deviations for each condition.

Motion ability of insects with thin films

A design strategy for mounting ultrathin films onto the abdomen was established that did not interfere with the basic motion of insects. Cross-sectional observation of the abdomen revealed that each segment partially overlapped during the deformation of the abdomen (Supplementary Fig. 5 and Supplementary Movie 1). The stroke of each segment was up to 2.5 mm. Freedom of movement of the abdomen was realised by using the combined technology of ultrathin polymer films and an adhesive–nonadhesive interleaving structure that allowed film bending (Fig. 2a). After attaching films on the abdomen with a resin adhesive, the adhesive can be naturally removed from the part that overlaps with other segments when deformed, and the film exhibits a hollow structure that selectively adheres only to the part that does not overlap. This adhesive–nonadhesive interleaving structure leaves space for the film to bend upward as the segment moves

(Supplementary Fig. 6 and Supplementary Movie 1). Similar outward bending was observed with parylene films of various thicknesses by using a 3D model mimicking the abdominal segments (Supplementary Fig. 7).

The effectiveness of the thin-film attachment strategy was quantified by measuring the time required to traverse an obstacle (Fig. 2b, c and Supplementary Movie 2). The fixed abdomen increased the required time for traversing the obstacles (2.4 s to 4.2 s as median values) (Fig. 2d). Whereas the 3 µm thick film with an adhesive–nonadhesive interleaving structure achieved approximately the same time of traversing as that with no film attached (median of 2.2 s). This shows that the fixation of each segment considerably impairs this deformability and limits motion and that the thin-film attachment strategy effectively secures the freedom of movement.

The effectiveness was further verified by evaluating the successful self-righting ability from an upside-down orientation on the ground (Fig. 2e, f). The righting success rate of *G. portentosa* with no films attached was 99%, which is consistent with previous results[30]. Thin films with various Young's moduli and thicknesses were attached to the abdomens of *G. portentosa*. When parylene films (Young's modulus of 4.0 GPa) were attached to the abdomen with an adhesive–nonadhesive interleaving structure, the righting success rates were 96 and 81% for the 5- and 10 µm thick films, respectively. For 15- and 20 µm thick films, the success rates were reduced to 46 and 16%, respectively (Supplementary Movie 3). A similar tendency was observed when soft polydimethylsiloxane (PDMS, Young's modulus of 3.3 MPa) was attached to the abdomen (Supplementary Fig. 8 and Supplementary Movie 4). By contrast, the righting success rate was 10% when the 2 µm thick parylene film was adhered to the abdomen without the interleaving structure. These results confirm that the combination of sufficiently thin film and the interleaving structure retains the mobility of the insects (Supplementary Fig. 9). Additionally, we confirmed the 3 µm thick parylene films with interleaving structure mounted on the insect did not falling off for at least 3 days.

Numerical relations between the abdominal conditions and the success rate of self-righting were detailed using an approximated buckling load model. The deformation of the film because of the stroke of an abdominal segment can be approximated by the buckling of a simple column fixed at both ends[31]. The buckling load can be obtained from the film thickness and Young's modulus of the film to be attached (Eqs. (1–3) in Methods, and Supplementary Fig. 10). The buckling loads were obtained as a function of the film thickness for both parylene and PDMS films using the given shape parameters of the abdominal segment (Supplementary Table 1) (Fig. 2g). The relationship between the buckling load and righting success rate exhibited consistency for both films, which confirmed the validity of the approximation (Fig. 2h). A buckling load of less than 0.05 N ensured a success rate of 80%, whereas further increment caused a sharp decrease in the rate. Thus, the force that abdominal segments of *G. portentosa* can generate range from 0.05 to 0.1 N, which is consistent with values with previously reported forces of legs during righting[32]. We conducted repeated self-righting attempts for an individual and for multiple individuals. Some individuals showed high success rate for multiple such attempts, whereas others showed 0% or very low success rate, confirming clear individual differences. The large error bars represent a boundary region that depends on the muscle strength of the individual.

The qualitative analysis of self-righting attempts confirmed that fundamental motion was achieved even when flexible electronics were integrated into insects (Fig. 2i, Supplementary Movie 5). When a 4 µm thick organic solar cell module was attached to the abdomen of a cockroach, 100% successful self-righting attempts were achieved, which confirmed that the ultrathin organic solar cell module ensured motion of insects. Unlike the adhesion of a thin film onto the abdomen, attaching a thick film (100 µm thick) with the support of the backpack on the thorax has a minor effect on self-righting ability. The success rate was 93% when the thorax

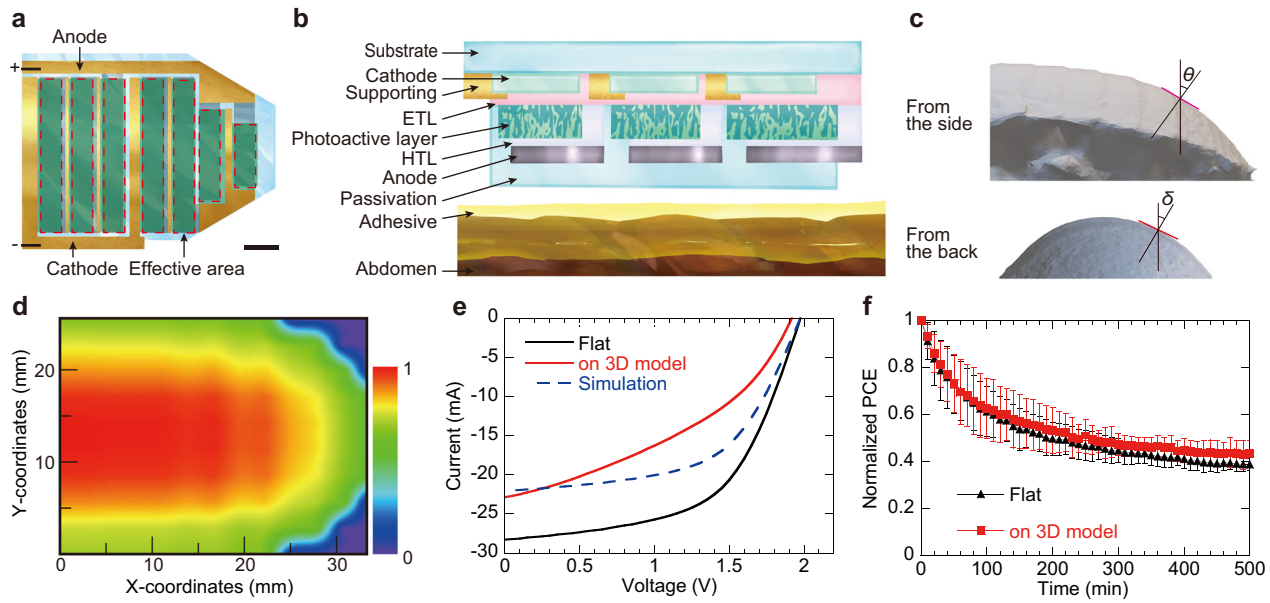

Fig. 3 Large-area organic solar cell module for cyborg insects. a Top view design of organic solar cell module. The dashed red lines indicate the effective area of the module. Scale bar, 5 mm. **b** Structure of the module. **c** Side and back views of the abdomen showing changes in the angle of light incident in each region. **d** Estimated distribution of light intensity changes in the abdomen. **e** Current–voltage (*I*–*V*) curves of the solar cell module measured under AM 1.5 G with 100 mW cm^{-2}. The black and red solid lines represent the measured performance on the flat stage and 3D printed curved surface, respectively. The dashed blue line represents the simulated curve from the distribution of the light intensity change. **f** Normalised PCE change with MPP tracking test time. Black triangles and red squares represent the module measured on the flat stage and 3D printed curved surface, respectively. Plots represent average values obtained from 5 individual modules, and the error bars represent standard deviation.

had a thick film, whereas the abdomen had no film. When 3 µm thick and 10 µm thick films were attached to the abdomen, the success rates were 80 and 13%, respectively. Thus, the results of the attempts with different conditions confirm that a relatively thick film can be mounted onto the thorax of *G. portentosa* to achieve fundamental motion, whereas the abdomen requires a film with a specific softness and a designed attachment strategy to allow sufficient deformation for motion.

Performance of ultrathin organic solar cell module

The ultrathin organic solar cell module achieves a high power output of up to 17.2 mW by maximizing the effective area of the curved surface shape of the abdomen of *G. portentosa* (Fig. 3a). The abdomen of *G. portentosa* was approximated as a pentagon with an area of 777 mm^2 (Supplementary Fig. 11). The module has a three-series connection considering the efficiency of the boosting converter (Fig. 3b). The effective area of the module was 3.96 cm^2, which corresponded to an aperture ratio of 51% to the abdominal area. Because the insect body has a three-dimensional curved surface, the light intensity that each cell can receive depends on the angle[25,33]. Based on the side and back shapes of the 3D model, the angles of the dorsal surface of *G. portentosa* with respect to the vertical line were set as θ and δ, respectively (Fig. 3c). The decrease in the light intensity in each region, that is, cos θ*cos δ, was estimated from both θ and δ in each region (Fig. 3d, Supplementary Fig. 12). The module was designed to minimise intensity reduction resulting from the angle dependence of the surface. Figure 3e shows the current–voltage (*I*–*V*) characteristics of the organic solar cell module. The flat ultrathin organic solar cell module exhibits a short current (I_{SC}) of 28.3 mA, an open-circuit voltage (V_{OC}) of 1.98 V, and a fill factor (FF) of 0.564, which resulted in a maximum power output of 31.5 mW, and PCE of 7.96% (Supplementary Table 2). The module attached on the 3D-printed curved surface model exhibits an I_{SC} of 22.8 mA, an open-circuit voltage (V_{OC}) of 1.92 V, and an FF of 0.394, which results in a maximum power output of 17.2 mW. The current decrement on the curved surface was estimated to be 0.78 times that of the flat state, which is in consistent with the actual current value when attached to the 3D surface (Fig. 3e, Supplementary Table 3 and Supplementary Fig. 13). The decrease in FF is related to the decrease in the shunt resistance because of the increase in the leakage current during the attachment process (Supplementary Fig. 14 and Supplementary Table 2).

The ultrathin solar cell has a weight per effective area of approximately 5 g m^{-2} [28], which corresponds to power per weight of 15.9 and 8.69 W g^{-1} for the large-area module on the flat state and on 3D-curved surface. The power density per effective area corresponds to 4.34 mW cm^{-2}. The smaller value of the module on the 3D-printed curved surfaces as compared to that of reported flexible organic solar cells (in which the highest power density per effective area was 17.5 mW cm^{-2})[34] originated from the decrement of the performance when the ultrathin devices were bent to 3D-shape. The output power generated by a soft solar cell module on the insect can be improved by suppressing the deterioration due to the process, improving instability under continuous light illumination, and design modification considering the specific curved surface of the target insects. Potential approaches include the use of an active layer material with a large optimal thickness[35], investigating stable interfacial materials[36], and the use of more mechanically robust materials for charge injection layers and transparent electrodes[37] as well as to use active layer materials showing higher power conversion efficiency[38].

We conducted the operation stability test of soft organic solar cell modules with both flat and attached on 3D model (Fig. 3f). Both modules on flat and on 3D model show similar operation stability under the maximum power point tracking (MPPT) of simulated sun-light, displaying the reasonable stability on curved surfaces. The faster degradation of the large area modules than small-area single cell is attributed from leakage current path of the larger effective area[28].

Charging wireless locomotion control system of living cyborg insect

The charging performance confirmed that the ultrathin organic solar cell module attached to the 3D-printed *G. portentosa* model could successfully supply power to the lithium–polymer battery. The voltage from the solar cell module to the input of the boosting converter was fixed at 0.95 V so that the module could be operated near the maximum power output point. The boosting converter increased the voltage from 0.95 to 4.2 V, and the output was used for charging the battery (Fig. 1d). The battery output voltage was increased from 3.13 to 4.33 V after charging for 938 min, which confirmed the charging was completed from empty to full (Fig. 4a).

The designed output signals for the stimulation were wirelessly controlled using a module with a negligible signal delay. Figure 4b displays the signal outputs for the electrical stimulation during wireless communication. When the switch on the external server was turned on, the stimulation circuit on the receiver produced a rectangular output voltage with a peak-to-peak voltage of 3.3 V, frequency of 50 Hz, and duty ratio of 50%. The delay times for both turn-on and turn-off ranged from 0.10 to 0.12 s.

Finally, recharging and wireless locomotion control was realised using living cyborg insects that contained electronic components (Supplementary Movie 6). The wireless locomotion control module, lithium–polymer battery, ultrathin organic solar cell module, and stimulus wires were attached to the dorsal side of *G. portentosa* (Fig. 1a, b). First, we confirmed that the stimulation was not applied before battery charging. After the simulated sunlight illumination was applied to the organic solar cell module on *G. portentosa* for 30 min, turn-right locomotion control was wirelessly conducted (Fig. 4c). The stimulation signals were wirelessly transmitted for 2.1 min with the charged battery. During this period, locomotion control was attempted multiple times, which confirmed that the wireless control was successfully performed repeatedly (Fig. 4d).

To allow freedom of motion, it is critical to separate the components between the thoracic and abdominal segments and ensure the freedom of the abdominal segments. The effectiveness of this design was quantitatively confirmed by evaluating the motions of the insect[39]. The insect's self-righting attempts succeeded when the attached thin film with an adhesive–nonadhesive interleaving structure was sufficiently soft to avoid disturbing the deformation force of the muscles of the insects. Such abdominal deformations have been observed in numerous insects[40,41]; therefore, the strategy of mounting flexible electronics proposed in this study can be adapted to other insect species. Considering the deformation of the thorax and abdomen during fundamental motion, hybrid electronic systems of rigid or flexible elements on the thorax and ultrasoft devices on the abdomen are effective cyborg insect designs.

Although the rigid circuits used in this study are not sufficiently thin and lightweight to ensure the full degree of freedom of *G. portentosa*, their thickness and weight can be reduced using precise and flexible circuits with organic semiconductors[9] and Si circuits fabricated on plastic films[42,43]. As demonstrated in this study, a circuit with a total thickness of up to 100 µm may provide nearly complete fundamental motion in *G. portentosa*. The thickness reduction of the circuit boards on the thorax should be the future direction of rechargeable cyborg insects.

Because the insects are constantly moving, the reduction of the angle dependence of power generation should be considered. The potential approach is to fabricate nano-grating structures onto the substrate or functional layers[25,33]. An interval of non-light illumination was needed for the charging

experiment to prevent the *G. portentosa* body temperature from rising too high, and cockroaches are generally nocturnal and photophobic. By integrating locomotion control system, photodiodes, and temperature sensors, an algorithm can be established that stimulates the cockroach to stay under the light during the charging mode of the system while considering life support. The measured power consumption of the wireless locomotion control system was 73.3 mW. The battery (40 mAh) lasted approximately 2 h after being fully charged. In the current system, most power consumption was used in wireless communication. By adjusting the communication intervals, the battery can last a longer time.

In conclusion, we established a design strategy for mounting electronics on insects through systematic evaluation of motion abilities and demonstrated charging and wireless locomotion control on living cyborg insects. Two critical strategies, namely achieving sufficient softness and a structure that ensures segment movement, minimise the reduction in the freedom of the body joints. The ultrathin organic solar cell module confirmed the effectiveness of the strategy by charging the battery on living movable insects. The separated functions of components on both the thorax and abdomen enabled sustained untethered usage of cyborg insects. This strategy is effective for other insects and device components. The approach presented in this study contributes to expand the range of activity and realises diverse functions for the cyborg insects.

METHODS

Experimental animals and breeding environment

Adult *G. portentosa* (over 16 weeks after birth) were used in this study. Their bodies can be divided into the head, thorax, and abdomen. From the top view, the head is mostly covered by the thorax. The thorax and the abdomen are further divided into three and eight segments, respectively.

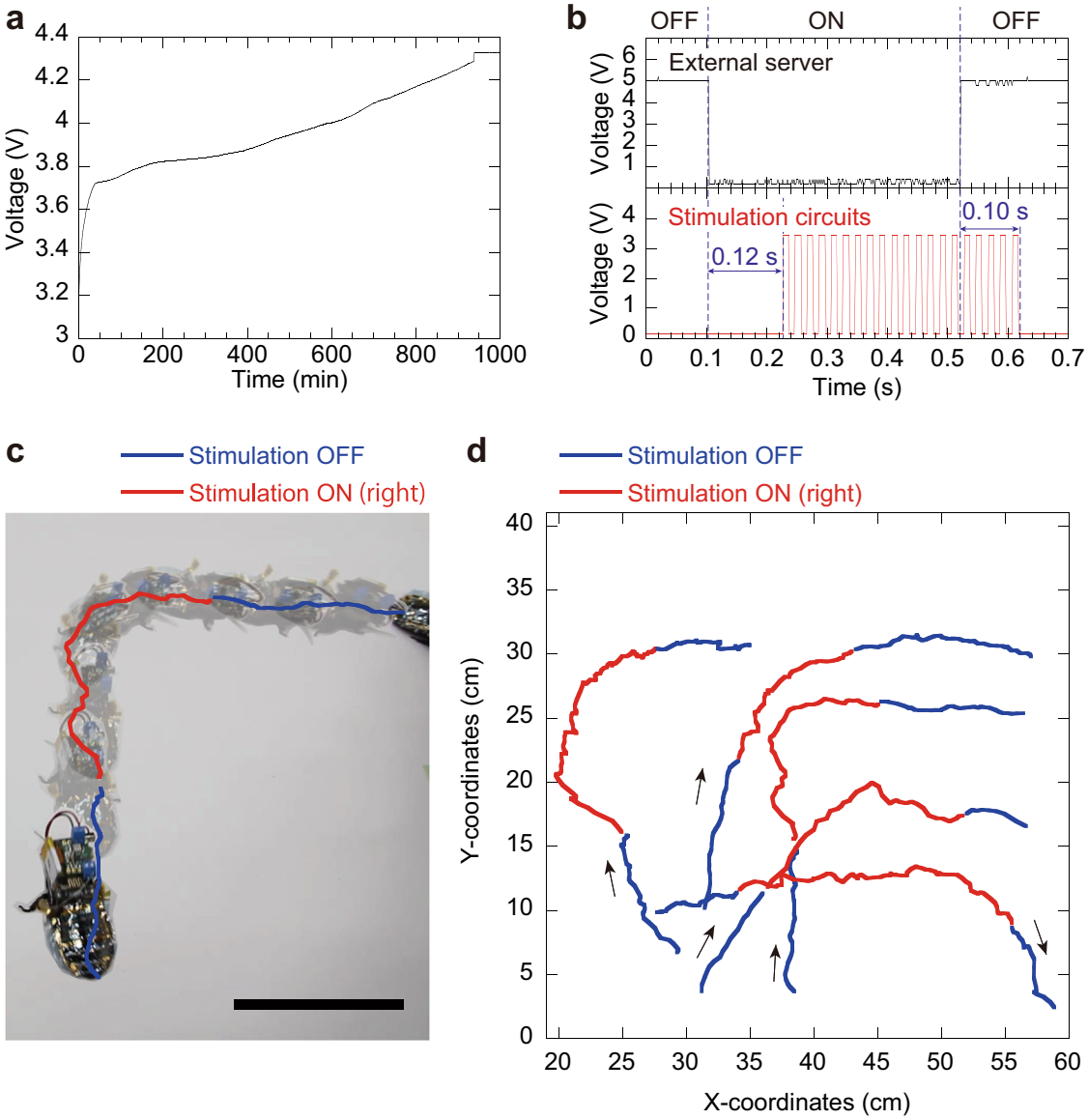

Fig. 4 Wireless locomotion control with recharged battery. a Charging of the battery using an organic solar cell module. The voltage between the batteries was plotted as a function of time during charging by an organic solar cell module attached to the 3D printed curved surface under AM 1.5 G with 100 mW cm^{-2}. **b** Voltage changes in the external server (top) and simulation module (bottom). When the switch was turned on, the signal was transmitted from the external server to the stimulation circuits, and stimulation waveforms were generated. **c** Multiple exposures and corresponding trajectories of locomotion. The blue and red lines represent off and on stimulation, respectively. Scale bar, 100 mm. **d** Trajectory of five locomotion control attempts.

Cerci are paired appendages on the rearmost segments of the abdomen and serve as sensory organs. Male *G. portentosa* can be distinguished by the presence of two horn-like protrusions on the thorax. To ensure uniform behavioural ability test conditions, only female individuals were used in the experiment to evaluate their self-righting ability with a film or backpack attached to the dorsal side. Commercially available bark chips were spread in a breeding case with a width of 43 cm, a depth of 35 cm, and a height of 27 cm for breeding 40 to 200 colonies. The breeding temperature was adjusted from 25 to 30 °C using a heater mat. Appropriate amounts of insect jelly and cockroach food were administered twice a week.

3D model of *G. portentosa*

A frozen *G. portentosa* female was placed on a small turntable, and 45 images were captured by rotating the specimen at 8° intervals. The images were imported into photogrammetry software (3DF Zephyr, OPT Technologies) to create a precise 3D model.

Abdominal shape measurement

An adhesive elastomer sheet (Y-4905J, 3 M ™) was tightly attached to the abdomen of a female *G. portentosa* specimen to fill the abdominal area. A paper was attached to the elastomer sheets to prevent deformation during delamination. The shape was determined with delaminated elastomer sheets and then approximated to a pentagon with a total area of 777 mm^2.

Confirmation of the abdominal movement and segment shape

Cross-sectional observation was performed to confirm the movement of the abdomen of *G. portentosa*. With a specimen frozen at −18 °C, a CO_2 laser processing machine (FABOOL Laser CO2, Smart DIYs Inc.) was used to cut *G. portentosa* from the centre of the thorax to the abdomen. Observations were conducted using a microscope (Dino-Lite Edge, Opto Science). The range of movement was measured using cross-sectional observation. The abdomen was disassembled into segments to measure the segment depth, width, thickness, and radius of curvature.

Design and fabrication of backpack

To achieve stable adhesion of rigid components on the thorax, the backpack was designed to cover the first to third thoracic segments of the 3D model of *G. portentosa*. The backpack was fabricated using a stereolithography 3D printer (Form3, Formlabs) with an elastic polymer (Elastic 50 A, Formlabs). The interface between the backpack and the insect surface was divided into columns. The columnar structures were attached to the first to third thoracic segments using a superglue (LOCTITE, LBR-005). Thanks to the softness and columnar structure, the backpack adhered to different individuals appropriately, confirming the adequate integration of circuits onto the *G. portentosa* species.

Attaching thin films to the abdomen

A resin-based adhesive for the skin (Spirit Gum, Mitsuyoshi) was evenly applied to the abdomen, and a thin film was attached to the surface of the insect. The adhesive was liquid and exhibited some adhesive strength even before curing. During the curing of the adhesive, the part of the adhesive where the segments overlapped was scraped off by the natural movement of the insects, which resulted in an adhesive–nonadhesive interleaving hollow structure.

Traversing an obstacle

A wooden regular triangular prism with a side and height of 45 and 80 mm was placed on the ground as an obstacle. The floor temperature at the initial position of *G. portentosa* was set to 80 °C, and the floor temperature of the obstacle and beyond the obstacle was set to room temperature (ranging from 23 to 25 °C) to trigger a traversal movement immediately. The traversal time was determined by measuring the time from when the head of *G. portentosa* passed through the nearest end face of the obstacle to when the abdomen sufficiently exceeded the top apex. We collected from a total of 5 individuals with 10 trials from each individual for each condition.

Self-righting attempts

G. portentosa was held in an upside-down orientation and then released on the ground covered with recycled paper. If the animal righted from an upside-down orientation within 60 s, the case was considered to be a success. The same attempts were repeatedly conducted with various individuals and film/component conditions on both the abdomen and thorax. We collected from a total of at least 3 individuals with at least 5 trials from each individual for each condition. See supplementary Table 4 for details of sample size.

Calculation of buckling load

Euler's formula for buckling load P is expressed as follows:

$$P = n\frac{\pi^2 EI}{L^2} \tag{1}$$

where n is a constant determined by fixing both ends of the sheet (in the case of both ends fixed, $n = 4$), E is the Young's modulus of the sheet, I is the moment of inertia of the area determined by the cross-sectional shape of the sheet, and L is the natural length between the fixed ends. The moment of inertia of the film area can be calculated using the following expression:

$$I = \frac{t^3 b}{12} \tag{2}$$

where t and b are the thicknesses and widths of the films. Therefore, the buckling load can be expressed as follows:[31]

$$P = \frac{\pi^2 Et^3 b}{4L^2} \tag{3}$$

Although the deformation between the two abdominal segments is vertical deviation, it is approximated to the buckling of a simple column with the stroke of the segment as L because the vertical deviation is sufficiently small (Supplementary Figs. 5 and 9). The force required for buckling deformation at a constant stroke of the abdominal segment ($L = 2.5$ mm) and film width on the abdominal segment ($b = 25$ mm) were calculated using Young's modulus and thickness as variables (Supplementary Table 1).

Materials for organic solar cell module

The precursor (ECRIOS VICT-Cz) for the transparent polyimide substrate was obtained from Mitsui Chemicals. The fluorinated polymers (Novec1700, 3 M) and their solvents (Novec 7100, 3 M) were purchased from 3 M. Zinc acetate dehydrates, ethanolamine, 2-methoxyethanol, and chlorobenzene were purchased from FUJIFILM Wako Pure Chemical Corporation. Ethoxylated polyethyleneimine (PEIE) and 1-chloronaphthalene were purchased from Sigma-Aldrich. Poly[4,8-bis(5-(2-ethylhexyl)thiophen-2-yl)benzo[1,2-b;4,5-b′] dithiophene-2,6-diyl-alt-(4-octyl-3-fluorothieno[3,4-b]thiophene)-2-carboxylate-2-6-diyl] (PBDTTT-OFT) was obtained from TORAY. 2,2′-((2Z,2′Z)-(((4,4,9,9-tetrakis(4-hexylphenyl)-4,9-dihydro-sindaceno[1,2-b:5,6-b′]dithiophene-2,7-diyl)bis(4-((2-ethylhexyl)oxy)thiophene-5,2-diyl))bis(methanylylidene))bis(5,6-difluoro-3-oxo-2,3-dihydro-1 *H*-indene-2,1-diylidene))dimalononitrile (IEICO-4F) was purchased from 1-Material. All the materials were used as received without further purification.

Fabrication of the organic solar cell module

First, the glass substrates were treated with an oxygen plasma for 10 min at 300 W (PC-300, Samco). The fluorinated polymer layer (Novec 1700:7100 = 1:8) was then spin coated (MS-B100, Miksa) on a 50 mm × 50 mm glass at 4000 rpm for 1 min. Next, the fluorinated glass substrate was heated in an inert oven at 80 °C for 10 min. Before spin coating the transparent polyimide precursor, the glass/fluorinated polymer layer was treated with an oxygen plasma for 5 s at 50 W. The precursor was spin coated onto the substrate at 2000 rpm for 1 min to form a film with a thickness of approximately 2.4 µm. The transparent polyimide film was cured by an imidisation reaction at 250 °C for 2 h in an inert oven under a nitrogen atmosphere (DN411I, Yamato Scientific). An indium tin oxide (ITO) transparent electrode with a thickness of 100 nm was deposited on the substrate using a sputtering machine (SIH-1010, ULVAC, Inc.). The ITO electrode was patterned by photolithography, and 3.5 nm-thick Cr and 100 nm-thick Au layers were deposited onto the ITO electrode as supporting wires. PEIE chelated with Zn^{2+} (PEI–Zn) was used as the electron transport layer[28,37]. The PEI–Zn precursor solution was prepared

by dissolving 70 mg of zinc acetate dihydrate in 1 wt% PEIE 2-methoxyethanol. To form the PEI–Zn film, the precursor solution was spin coated at 3500 rpm for 45 s and subsequently thermally annealed at 180 °C for 30 min in air. PBDTTT-OFT (10 mg) and IEICO-4F (15 mg) in chlorobenzene (970 µL) were heated at 70 °C for 2 h. The additive, 1-chloronaphthalene (30 µL), was added to the solution and stirred at 70 °C for 5 min. The solution was spin coated in ambient air at 1400 rpm for 60 s to form a bulk heterojunction photoactive layer. Unnecessary areas were carefully removed using a cotton swab soaked in chloroform to connect each sub-cell in series. The dried samples were placed in a vacuum evaporator, and a hole-transporting layer of molybdenum oxide (MoO_X, 7.5 nm) and an Ag anode (100 nm) were sequentially deposited through thermal evaporation at $<3 \times 10^{-4}$ Pa. Finally, a 1 µm-thick parylene layer was deposited through chemical vapor deposition to form a passivation layer. The solar cell module has three series and two parallel subcells with an effective area of 22×3 mm. The total effective area was 396 mm^2, which corresponded to 51% of the aperture ratio of the abdominal area of *G. portentosa* (777 mm^2).

Module characterisation

The current–voltage (*I*–*V*) characteristics of the OPVs were recorded under AM 1.5 G (100 mW cm^{-2}, with the intensity calibrated using a silicon reference solar cell) using a SourceMeter (Series2400, Keithley) under ambient laboratory conditions.

Wireless locomotion control module and battery

The wireless locomotion control module consisted of three rigid components, namely a stimulation voltage generation circuit, wireless communication circuit, and boosting converter. To receive the on/off status from the external server, a wireless communication module with nRF24L01 + (Nordic Semiconductor) was used. An Arduino Pro mini was used as the stimulus voltage generation circuit. For electrical stimulation of *G. portentosa*, pulse-width modulation control was programmed to produce a signal with 3.3 V, 50 Hz, and duty ratio of 50%. An energy-harvesting IC (LTC3105 250 mV low voltage boosting converter module, Strawberry Linux Co., Ltd.) was installed to stably charge the battery using the output from the organic solar cell module. The output power from the organic solar cell module was fixed at 0.95 V using a maximum power point controller with a 100 kΩ resistor, and the boosting converter increased the voltage to 4.2 V. A 3.7 V, 40 mAh lithium–polymer battery was used as the rechargeable battery. The overall dimensions of these components were W 18.0 mm × L 37.2 mm × H 18.3 mm, and the weight was 8.14 g, and these were mounted onto the thorax with the 3D-printed backpack.

An Arduino Uno external server was used as the microcomputer board. A communication module equipped with an nRF24L01 + (Nordic Semiconductor) was used as the wireless module for communication. Furthermore, an Arduino Uno with a push-button switch was used to control the on/off state. The state of this button was transmitted to the module on the insect through a wireless communication module. The external server was connected to a PC to obtain a constant voltage of 5 V.

Charging test

The lithium–polymer battery was discharged to 3.2 V using an electrochemical measurement system (HZ-7000, Hokuto Denko). The organic solar cell module attached to the 3D printed *G. portentosa* model was connected to the battery. The simulated 1-Sun light was applied continuously to the module directly from above, and the voltage between the batteries was monitored using a source meter (Series2400, Keithley).

Mounting of electric components onto the insect

The surfaces of the thoracic and abdominal segments of *G. portentosa* were scraped evenly with sandpaper. The 3D printed backpack was attached to the first to third thoracic segments using a superglue (LOCTITE, LBR-005). The wireless locomotion control module and battery were attached to the backpack using a double-sided tape (Nystack™ NW-5, Nichiban Co., Ltd.). Holes were made on the side of the fifth abdominal segment and cerci using an insect needle (No. 1, Shiga Insect Spreading Co., Ltd.) or a scalpel. Silver microwires were connected to the holes and fixed using an ultraviolet curing epoxy resin (UV-LED resin star drop hard, Padico). An ultrathin organic solar cell module was attached to the whole abdomen using a resin-based adhesive for skins (Spirit Gum, Mitsuyoshi). Both the anodes and cathodes were connected to boosting converters using an anisotropic conductive tape (ECATT 9703, 3 M) and silver microwires.

Demonstration of recharging and wireless locomotion control of cyborg insect

A simulated 1-Sun light was applied to *G. portentosa* to recharge the empty battery using a solar cell module. The total illumination duration was 30 min. A 2 min interval was set for every 10 min illumination to prevent the *G. portentosa* body temperature from rising too high. After the recharging process, a wireless electrical stimulation test was performed. When electrical stimulation was applied to the right cercus, the insect made the turn-right locomotion. The time during which the control server and the electrical stimulation module communicated was measured to evaluate the total energy provided to the battery by the organic solar cell module. To confirm whether electrical stimulation achieved effective control, the trajectory of the rear end of *G. portentosa* was recorded using a video camera and analysed using MATLAB (The MathWorks).

DATA AVAILABILITY

Source data are provided with this paper.

CODE AVAILABILITY

All code for the stimulation module is provided in the supplementary information.

Received: 6 June 2022; Accepted: 27 July 2022;
Published online: 05 September 2022

REFERENCES

1. Warwick, K. Cyborg morals, cyborg values, cyborg ethics. *Ethics Inf. Technol.* **5**, 131–137 (2003).
2. Tran-Ngoc, P. T. et al. Insect-computer hybrid system for autonomous search and rescue mission. Preprint at https://arxiv.org/abs/2105.10869 (2021).
3. Latif, T., Whitmire, E., Novak, T. & Bozkurt, A. Sound localization sensors for search and rescue biobots. *IEEE Sens. J.* **16**, 3444–3453 (2016).
4. Cao, F. et al. A biological micro actuator: Graded and closed-loop control of insect leg motion by electrical stimulation of muscles. *PLoS One* **9**, e105389 (2014).
5. Erickson, J. C., Herrera, M., Bustamante, M., Shingiro, A. & Bowen, T. Effective stimulus parameters for directed locomotion in Madagascar Hissing Cockroach Biobot. *PLoS One* **10**, e0134348 (2015).
6. Sato, H. & Maharbiz, M. M. Recent developments in the remote radio control of insect flight. *Front. Neurosci.* **4**, 199 (2010).
7. Tsang, W. M. et al. Insect-machine interface: A carbon nanotube-enhanced flexible neural probe. *J. Neurosci. Methods* **204**, 355–365 (2012).
8. Gao, W. et al. Fully integrated wearable sensor arrays for multiplexed in situ perspiration analysis. *Nature* **529**, 509–514 (2016).
9. Kim, Y. et al. A bioinspired flexible organic artificial afferent nerve. *Science* **360**, 998–1003 (2018).
10. Kwon, K. et al. An on-skin platform for wireless monitoring of flow rate, cumulative loss and temperature of sweat in real time. *Nat. Electron.* **4**, 302–312 (2021).
11. Lee, S. et al. Nanomesh pressure sensor for monitoring finger manipulation without sensory interference. *Science* **370**, 966–970 (2020).
12. Matsuhisa, N. et al. High-frequency and intrinsically stretchable polymer diodes. *Nature* **600**, 246–252 (2021).
13. Jung, D. et al. Highly conductive and elastic nanomembrane for skin electronics. *Science* **1026**, 1022–1026 (2021).
14. Jun, S., Lee, S. & Yih, Y. Pickup and delivery problem with recharging for material handling systems utilising autonomous mobile robots. *Eur. J. Oper. Res.* **289**, 1153–1168 (2021).
15. Kurs, A. et al. Wireless power transfer via strongly coupled magnetic resonances. *Science* **317**, 83–86 (2007).
16. Huang, J., Zhou, Y., Ning, Z. & Gharavi, H. Wireless power transfer and energy harvesting: Current status and future prospects. *IEEE Wirel. Commun.* **26**, 163–169 (2019).
17. Shi, B., Li, Z. & Fan, Y. Implantable energy-harvesting devices. *Adv. Mater.* **30**, 1801511 (2018).
18. Jafferis, N. T., Helbling, E. F., Karpelson, M. & Wood, R. J. Untethered flight of an insect-sized flapping-wing microscale aerial vehicle. *Nature* **570**, 491–495 (2019).

19. Cosnier, S., le Goff, A. & Holzinger, M. Towards glucose biofuel cells implanted in human body for powering artificial organs: Review. *Electrochem. Commun.* **38**, 19–23 (2014).
20. Shoji, K. et al. Biofuel cell backpacked insect and its application to wireless sensing. *Biosens. Bioelectron.* **78**, 390–395 (2016).
21. Shoji, K., Morishima, K., Akiyama, Y., Nakamura, N. & Ohno, H. Autonomous environmental monitoring by self-powered biohybrid robot. In *2016 IEEE Int. Conf. Mechatron. Autom*. 629–634 (2016).
22. Liu, Y., Pharr, M. & Salvatore, G. A. Lab-on-skin: A review of flexible and stretchable electronics for wearable health monitoring. *ACS Nano* **11**, 9614–9635 (2017).
23. Latif, T., Whitmire, E., Novak, T. & Bozkurt, A. Towards fenceless boundaries for solar powered insect biobots. In *Proc. Annu. Int. Conf. IEEE Eng. Med. and Biol. Soc.* 1670–1673 (2014).
24. Latif, T. & Bozkurt, A. Line following terrestrial insect biobots. In *Proc. Annu. Int. Conf. IEEE Eng. Med. and Biol. Soc*. 972–975 (2012).
25. Park, S. et al. Self-powered ultra-flexible electronics via nano-grating-patterned organic photovoltaics. *Nature* **561**, 516–521 (2018).
26. Kaltenbrunner, M. et al. Flexible high power-per-weight perovskite solar cells with chromium oxide–metal contacts for improved stability in air. *Nat. Mater.* **14**, 1032–1039 (2015).
27. Zhang, X., Öberg, V. A., Du, J., Liu, J. & Johansson, E. M. J. Extremely lightweight and ultra-flexible infrared light-converting quantum dot solar cells with high power-per-weight output using a solution-processed bending durable silver nanowire-based electrode. *Energy Environ. Sci.* **11**, 354–364 (2018).
28. Xiong, S. et al. Ultrathin and efficient organic photovoltaics with enhanced air stability by suppression of Zinc element diffusion. *Adv. Sci.* **9**, 2105288 (2022).
29. Full, R. & Ahn, A. Static forces and moments generated in the insect leg: comparison of a three-dimensional musculo-skeletal computer model with experimental measurements. *J. Exp. Biol.* **198**, 1285–1298 (1995).
30. Li, C., Wöhrl, T., Lam, H. K. & Full, R. J. Cockroaches use diverse strategies to self-right on the ground. *J. Exp. Biol.* **222**, jeb186080 (2019).
31. Timoshenko, S. & Gere, J. M. *Theory of Elastic Stability*. (McGraw-Hill Book Company, Inc., 1961).
32. Full, R., Yamauchi, A. & Jindrich, D. Maximum single leg force production: cockroaches righting on photoelastic gelatin. *J. Exp. Biol.* **198**, 2441–2452 (1995).
33. Takakuwa, M. et al. Nanograting structured ultrathin substrate for ultraflexible Organic photovoltaics. *Small Methods* **4**, 1900762 (2020).
34. Zeng, G. et al. Realizing 17.5% efficiency flexible organic solar cells via atomiclevel chemical welding of Silver Nanowire Electrodes. *J. Am. Chem. Soc.* **144**, 8658–8668 (2021).
35. Vohra, V. et al. Efficient inverted polymer solar cells employing favourable molecular orientation. *Nat. Photon.* **9**, 403–408 (2015).
36. Li, Y. et al. Non-fullerene acceptor organic photovoltaics with intrinsic operational lifetimes over 30 years. *Nat. Commun.* **12**, 5419 (2021).
37. Qin, F. et al. Robust metal ion-chelated polymer interfacial layer for ultraflexible non-fullerene organic solar cells. *Nat. Commun.* **11**, 4508 (2020).
38. Zhu, L. et al. Single-junction organic solar cells with over 19% efficiency enabled by a refined double-fibril network morphology. *Nat. Mater.* **21**, 656–663 (2022).
39. Ritzmann, R. E., Quinn, R. D. & Fischer, M. S. Convergent evolution and locomotion through complex terrain by insects, vertebrates and robots. *Arthropod Struct. Dev.* **33**, 361–379 (2004).
40. Liang, Y. et al. Kinematics of Stewart Platform explains three-dimensional movement of Honeybee's abdominal structure. *J. Insect Sci.* **19**, 1–6 (2019).
41. Frantsevich, L. Righting kinematics in beetles (Insecta: Coleoptera). *Arthropod Struct. Dev.* **33**, 221–235 (2004).
42. Kim, D.-H. et al. Dissolvable films of silk fibroin for ultrathin conformal bio-integrated electronics. *Nat. Mater.* **9**, 511–517 (2010).
43. Yokota, T. et al. A conformable imager for biometric authentication and vital sign measurement. *Nat. Electron.* **3**, 113–121 (2020).

ACKNOWLEDGEMENTS

This work was partially supported by the Japan Society for the Promotion of Science under its Grants-in-Aid for Scientific Research (KAKENHI) (no. JP18H05469), and Japan Science and Technology Agency (JST) under its Adaptable and Seamless Technology Transfer Program through Target-driven R&D (A-STEP) (no. A3015021R), and JST under its JST-Mirai Program (no. JPMJMI21I1). We thank Toray Industries, Inc., for supplying the PBDTTT-OFT polymer. We thank Mitsui Chemicals for supplying transparent polyimide precursors (ECRIOS^{TM}).

AUTHOR CONTRIBUTIONS

S.U., H.S., Ke.F., and T.S. conceived of the main idea. Y.K., S.K., and Ke.F. designed and conducted experiments. Y.K., S.L., and M.T. fabricated the organic solar cell modules. Y.K., S.K. and Ke.F. analysed the data. Ke.F. and Ka.F. calculated the mechanics of a film using an approximation model. Y.K., S.K., Ke.F. T.S. wrote the manuscript. Ke.F. and T.S. supervised the project.

COMPETING INTERESTS

The authors declare no competing interests.

ADDITIONAL INFORMATION

Supplementary information The online version contains supplementary material available at https://doi.org/10.1038/s41528-022-00207-2.

Correspondence and requests for materials should be addressed to Kenjiro Fukuda or Takao Someya.

Reprints and permission information is available at http://www.nature.com/reprints

Publisher's note Springer Nature remains neutral with regard to jurisdictional claims in published maps and institutional affiliations.